Sensors and Actuators A 270 (2018) 205–213

Contents lists available at ScienceDirect

Sensors and Actuators A: Physical

journal homepage: www.elsevier.com/locate/sna

Fibre-optic temperature and pressure sensor based on a deformable concave micro-mirror

Abdelhak Guermat[a,b], Assia Guessoum[a], Nacer-Eddine Demagh[a,*], Monsef Zaboub[a], Zaied Bouhafs[a]

[a] Laboratoire d'Optique Appliquée [Applied Optics Laboratory], Institut d'Optique et Mécanique de Précision [Institute of Optics and Precision Mechanics, Ferhat Abbas University Setif1, Setif, Algeria], Université Ferhat Abbas Sétif 1, Algerie

[b] Unité de recherche en optique et photonique, UROP – CDTA, [Optics and Photonics Research Unit, Ferhat Abbas Setif1, Setif, Algeria], Université Ferhat Abbas Sétif 1, Sétif, Algerie

ARTICLE INFO

Article history:
Received 15 September 2017
Received in revised form
30 December 2017
Accepted 2 January 2018
Available online 2 January 2018

Keywords:
Fibre optic sensors
Pressure
Temperature
Amplitude modulation
PDMS
Micro-mirror

ABSTRACT

This article presents a fibre-optic sensor that measures temperature and pressure. Its operating principle is based on the amplitude modulation caused by the variation in the radius of a concave micro-mirror crafted into the end of an SMF optical fibre. In fact, a micro-cavity engraved into the end of the fibre by selective chemical etching is filled with a PDMS (Polydimethylsiloxane)-type polymer. Due to surface tension, the polymer micro-drop takes on a hemispheric shape characterised by a certain radius. After polymerisation in an oven at 100 °C for one hour, the hemispheric micro-drop is coated with a thin layer of gold using the vacuum evaporation technique. Typically, concave micro-mirrors can be obtained with bend radii of between 10µm and 30µm. Under the action of a temperature gradient or a variation in pressure, the thickness of the PDMS changes and causes a variation in the bend radius of the micro-mirror. As a result, the light intensity guided by the optical fibre and reflected by the micro-mirror is modulated by the variation in its bend radius. In this configuration, the sensor has a thermo-sensitivity of – 0.08dB/°C with a resolution of 0.13 °C in a range of between 20 °C and 100 °C. It also has a pressure sensitivity of 0.11dB/bar between 10 and 20 bars. The measurements are taken by a reflectometer (OTDR). In addition, the experimental results have been validated by theoretical modelling. This sensor is relatively simple to make and can be used in a wide range of applications, in particular biomedical and industrial ones.

1. Introduction

Fibre optic sensors are widely used in many fields due to their advantages with respect to miniaturisation, sensitivity, thermal stability, immunity to electromagnetic interference and ergonomics [1,2]. Their scope of application includes the fields of biomedicine [3,4], biochemistry [5,6], industry [7,8] aerospace [9] and security [10].

In metrology, the sensors are used to measure physical parameters such as temperature [11–18], pressure [19–24], stress [25–30], refraction index [31–37], vibrations [38–40], micro-movements [41–44], water salinity [45] and other parameters. The simultaneous measurement of two physical parameters, in this case temperature and pressure, are somewhat difficult as they are coupled [46]. These parameters are often determined by phase modulation fibre-optic sensors, notably interferometers such as Michelson [47,48], Mach-Zehnder [49,50], FBG (Fibre Bragg Grating) [51,52] and Fabry-Pérot (FPI) [53–56]. Their use is relatively complex because they generally require coherent sources [57]. On the other hand, amplitude-modulation fibre-optic sensors [58–63] are somewhat less expensive and easier to use [64].

With respect to the temperature and pressure measurements, interferometric sensors have the best performance and have undergone wide-scale prospecting and development studies. Xuan-Yu Zhang et al [65] have proposed an FPI configuration in which they obtained a sensitivity of 0.385 nm/°C between 25 °C and 60 °C with a resolution of 0.01 °C. The latter's results are consistent with those of Min Li et al [66], who obtained a sensitivity of 0.38052 nm/°C in a range of from 25 °C to 55 °C with a resolution of 0.05 °C. X. L. Tan et al [67] designed another variant with improved sensitivity, namely 0.19 nm/°C at a temperature interval of from 25° to 65 °C. Jing Kong

* Corresponding author.
E-mail addresses: aguermat@cdta.dz (A. Guermat), assiademagh@univ-setif.dz (A. Guessoum), ndemagh@univ-setif.dz (N.-E. Demagh), monsefzaboub@univ-setif.dz (M. Zaboub), zaiedbouhafs@univ-setif.dz (Z. Bouhafs).

https://doi.org/10.1016/j.sna.2018.01.001
0924-4247/

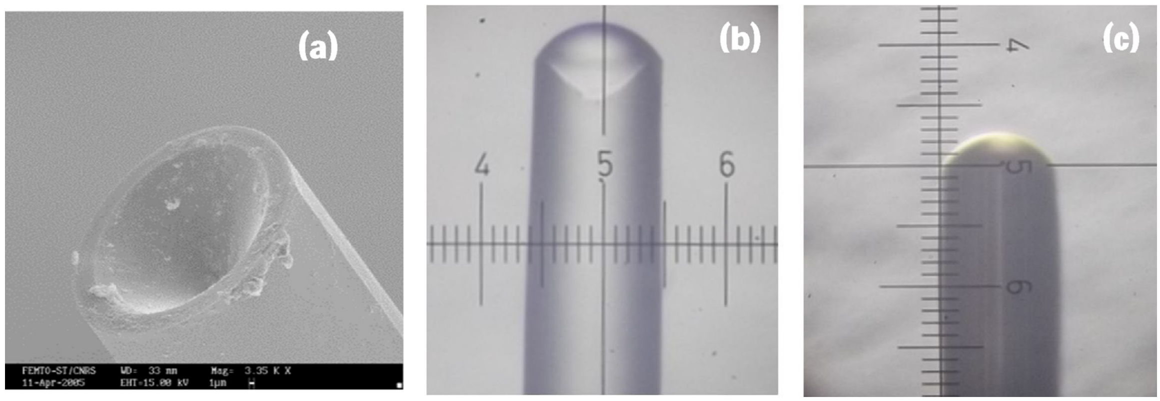

Fig. 1. Fabrication of a micro-mirror at the end of an SMF fibre: (a) Magnified view of the conical micro-cavity; (b) Fulfilled micro-cavity with PDMS; (c) Achieved deformable micro-mirror.

et al [68] have built a sensor that operates in a larger temperature interval of from 20 °C to 100 °C with a sensitivity of 0.079 nm/m^{-1}. With the same FPI configuration but for the pressure measurement, Shen Lieu et al [69] obtained a sensitivity of 43.4 nm/MPa for an interval of 0 to 2.0 MPa. W. P. Chen et al [70], optimised the sensitivity to -40.94 nm/MPa but in a relatively shorter interval of 0 to 0.92 MPa with a gradient of 0.04 MPa. Ben Xu et al [71] have also proposed an FPI configuration operating between 0 and 1.52 MPa with a sensitivity of 4.147nm/MPa.

Where temperature and pressure are measured simultaneously, Bing Sun et al [72] presented a sensor operating in a temperature range of from 40 °C to 90 °C, and a pressure range of 0.1 to 2.5 MPa. The sensor sensitivity obtained is from 0.249 nm/°C for temperature and 1.130 nm/MPa for pressure.

In the category of amplitude modulation sensors, Husna Abdul Rahman et al [73] have made an active temperature sensor in a range of 42 °C to 90 °C with a sensitivity of 0.0044 mV/ °C and a resolution of 2.4 °C. To measure displacement, S. W. Harun et al [74] presented a configuration enabling measurement at an interval of 0–4 mm with a sensitivity of 0.299 mV/μm. Regarding micro-displacements, Chen Yang et al [63] obtained a sensitivity of 0.36 mV/μm for a 50 nm displacement.

The sensor proposed in this work is based on the modulation of the reflected light intensity produced by the deformation of a concave micro-mirror crafted at the end of a single-mode SMF optical fibre. It can be used as a temperature sensor or a pressure sensor.

A calculation based on coupling efficiency η has been developed to study the performance of the sensor. In addition, we show that the results obtained through modelling are consistent with the experimental results.

2. Sensors fabrication

The sensor is composed of a single-mode SMF fibre (9/125 μm) equipped on the end with a flexible micro-mirror. Its manufacture takes place in three steps as shown in Fig. 1. First, a conical micro-cavity is engraved into the end of this fibre using the selective chemical etching technique with hydrofluoric acid HF (40%) [75]. The dimensions of this microstructure are checked in real time using a system of image acquisition and processing in association with a microscope. Depending on the immersion time, we typically obtain micro-cavities with depths of up to ~38μm and base widths of ~40μm. The micro-cavity is then filled with a micro-drop of PDMS polymer (Silgar 134 polydimethylsiloxane) using an automated micro-syringe with controlled flow (Graseby 3100 Syringe Pump). Because of the superficial tension forces [4], a hemispheric surface Fig. 1(b) with a bend radius that depends on the amount of polymer injected and the width of the conical micro-cavity [76] is formed. This end component is then polymerised in an oven at 100 °C for one hour.

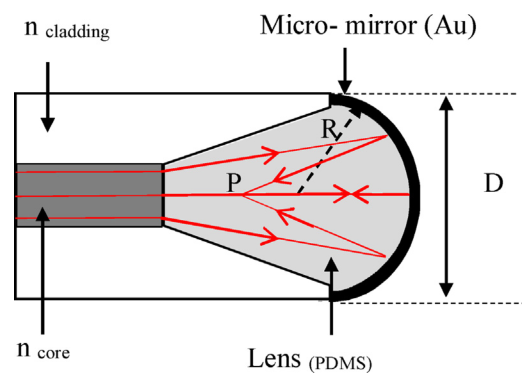

Fig. 2. Illustration of the sensor's operating principle.

To make the reflecting mirror, the hemispheric surface is covered with a thin layer of gold 100 nm thick, deposited using the vacuum evaporation technique. The gold layer acts as a protective coating and as the flexible reflecting mirror Fig. 1(c).

3. Principle of operating

The principle of the sensor is shown in Fig. 2. The light guided into the core of the SMF fibre through the micro-cavity containing the PDMS is projected onto the concave micro-mirror. The latter reflects the incident light and focuses it on a point P on the axis of the fibre. The part of the beam contained in the angle of acceptance of the fibre is reflected and carried by the fibre to the sensor.

The sensor's operation is based on the deformation of the micro-mirror under the effect of the local variations in temperature and pressure. When the physical conditions vary, the polymer in the micro-cavity dilates and contracts, which varies the bend radius R of the micro-mirror. Consequently, the focal point P is displaced on axis *z*. The deformation can still be reversed in the elastic part of the material in accordance with the PDMS characteristics shown in Table 1.

3.1. Thermal effect on the micro-mirror

The thermal effect on the sensor is shown in the pictures in Fig. 3. When the sensor is subjected to a rise in temperature, a decrease in the radius of curvature can be seen. Fig. 3(a) and (b) show the bend in the micro-mirror indicated by dotted circular arcs. The bend radius obtained is 75 μm at 20 °C and increases by 27 μm to 85 °C.

Table 1
Properties of the PDMS [77–81].

Properties of the PDMS (10:1)	Values
Lineal thermal expansion coefficient α.	4.71×10^{-4} K^{-1}
Thermo-optic expansion ratio ξ.	-4.66×10^{-4} K^{-1}
Refraction index n.	1.418
Temperature range.	−50 °C + 200 °C
Young E. modulus	750 kPa
Poisson's ratio	0.5
Density	920 Kg/m^3
Yield strength (σ)	20kPa

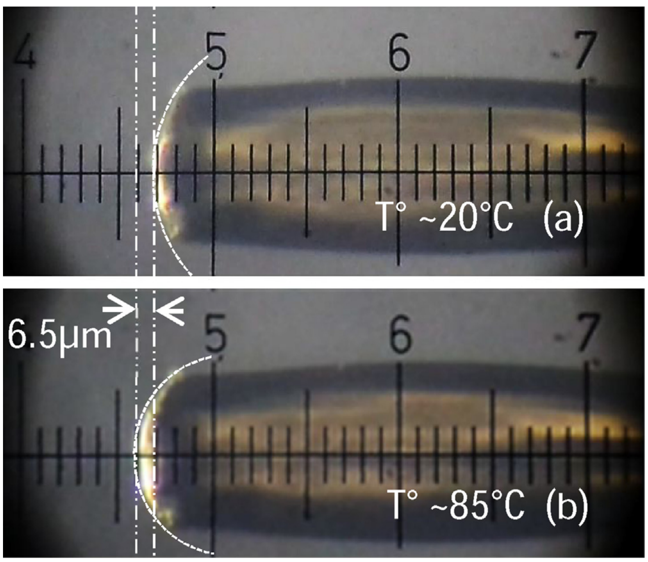

Fig. 3. Side views showing the bend in the micro-mirror at 20 °C and 85 °C.

Thermal dilatation has caused a 6.5 μm axial deformation of the micro-mirror.

4. Analysis

4.1. Calculation of the coupling parameters

The Thermal action and pressure on the PDMS can be analysed in terms of the efficiency of the given coupling by the coupling coefficient η. The latter represents the ratio of the light intensity reflected on the incident intensity. The coupling efficiency [82] is written as the following formula,

$$\eta = \frac{\left| \iint \psi_r \psi_f^* d_x d_y \right|^2}{\iint |\psi_r|^2 d_x d_y \iint |\psi_f|^2 d_x d_y} \tag{1}$$

In which ψ_r indicates the electrical field of the beam reflected by the mirror and ψ_f the field of the essential mode of the SMF optical fibre.

In the case under consideration (Fig. 4), the equation Eq. (1) can be written with respect to the beam waist object ω_0 and the beam waist image ω_{01} as the following formula [83],

$$\eta = \frac{2\omega_{01}\omega_0}{\sqrt{(\omega_{01}^2 + \omega_0^2)^2 + \frac{\lambda^2 z^2}{\pi^2}}} \tag{2}$$

in which ω_0 indicates the radius of fundamental mode of the SMF fibre which is determined using the Marcuse equation [84]. At the wavelength λ = 1.55 μm, ω_0 = 5.2 μm. The radius of the waist image ω_{01} formed at distance *z* from the waist objet is determined by applying the ABCD law [85].

The ABCD law is based on the calculation of the transfer matrix M_T of the optical system. In the case under consideration, the matrix can be broken down into three matrices M_{12}, M_{23} et M_{34}designating, respectively, the progress of the beam through the medium (PDMS) from position 1 to position 2, from 2 to 3, and finally from 3 to 4. Thus, we obtain the formula,

$$M_T = M_{34} M_{23} M_{12} = \begin{bmatrix} A & B \\ C & D \end{bmatrix} \tag{3}$$

in which A, B, C, and D are the elements of the matrix to be defined.

In addition, the formulae for the elementary matrices are:

$$M_{12} = \begin{bmatrix} 1 & \frac{d}{n} \\ 0 & 1 \end{bmatrix}, M_{23} = \begin{bmatrix} 1 & 0 \\ \frac{-2}{R} & 1 \end{bmatrix}, M_{34} = \begin{bmatrix} 1 & \frac{z_\omega}{n} \\ 0 & 1 \end{bmatrix} \tag{4}$$

in which $d = z + z_\omega$ is the distance between the end of the concave mirror and the surface of the core of the optical fibre and z_ω is the working distance.

The radius of bend R of the PDMS is calculated with respect to the diameter D of the micro-mirror and thickness h. It is given by the following ratio,

$$R = \frac{1}{2h}\left(h^2 + \frac{D^2}{4}\right) \tag{5}$$

The calculation of the total transfer matrix is thus written as the following formula.

$$M_T = \begin{bmatrix} 1 - \frac{2}{nR} z_\omega & \frac{d\left(1 - \frac{2z_\omega}{nR}\right)}{n} + \frac{z_\omega}{n} \\ \frac{-2}{R} & 1 - \frac{2}{nR} d \end{bmatrix} \tag{6}$$

in which one deduces the four elements of the matrix which are written as follows:

$$A = 1 - \frac{2}{nR} z_\omega, \; B = \frac{d\left(1 - \frac{2z_\omega}{nR}\right)}{n} + \frac{z_\omega}{n}, \; C = \frac{-2}{R}, \; D = 1 - \frac{2}{nR} d.$$

The waist image $2\omega_{01}$ and the working distance z_ω are calculated, respectively based on Eqs. (7) and (8) below [86].

$$\omega_{01} = \omega_0 \left[\frac{A^2 + a^2 B^2}{AD - BC} \right]^{1/2} \text{where } a = \frac{\lambda}{n_{PDMS} \pi \omega_0^2} \tag{7}$$

$$AC + a^2 BD = 0 \tag{8}$$

We therefore obtain the following formulae:

$$z_\omega = \frac{2n^2R^2 + 2a^2d^2nR - a^2RdnR^2}{4Rn^2 + 4a^2d^2R - 4a^2dR^2n + a^2nRR^2} \tag{9}$$

$$\omega_{01} = \sqrt{\omega_0\left(\frac{R^2n^2 + 4n^2z_\omega R + 4n^2{z_\omega}^2 + a^2d^2R^2 + 4a^2d^2Rz_\omega + 2a^2dR^2z_\omega + 4a^2d^2{z_\omega}^2 + 4a^2d{z_\omega}^2R + a^2{z_\omega}^2R^2}{n^2R^2}\right.}} \tag{10}$$

The coupling efficiency η can be determined by introducing ω_0 and ω_{01} in Eq. (2). We obtain the formula

$$\eta = \frac{2\omega_{01}\omega_0}{\sqrt{(\omega_{01}^2 + \omega_0^2)^2}} \tag{11}$$

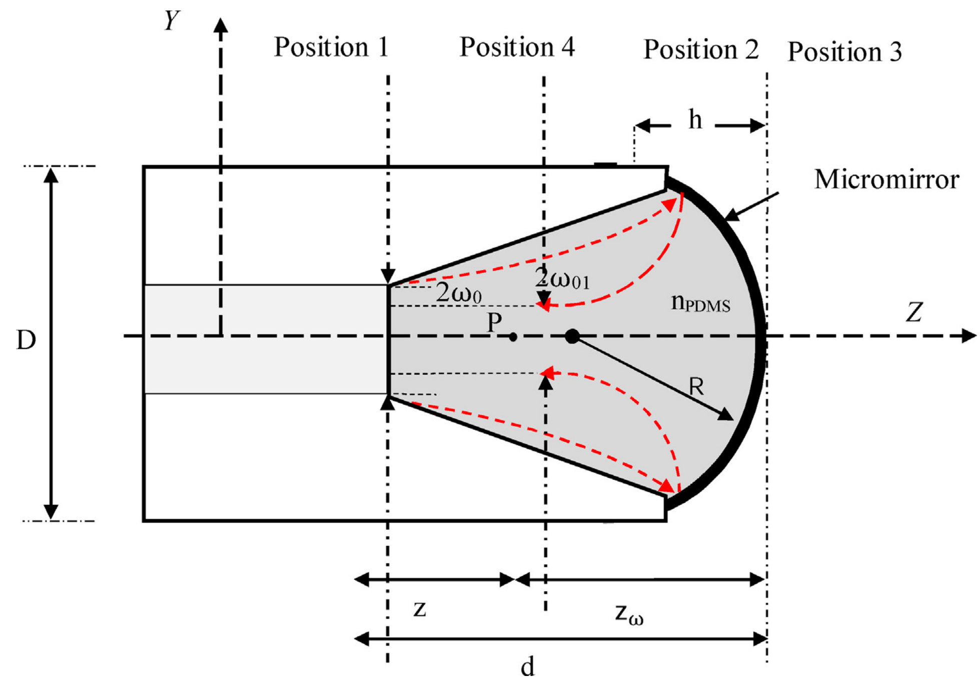

Fig. 4. Illustration of the operating principle of the micro-mirror.

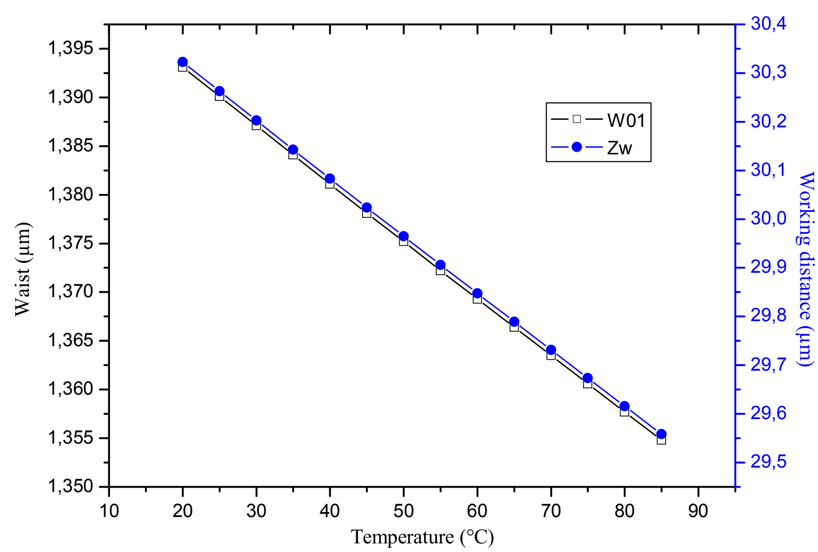

Fig. 5. Variation in the waist with respect to the bend radius.

4.2. Thermal effect on the coupling efficiency η(T)

The thermal effect, which causes a variation in the thickness h of the PDMS, can be formulated with respect to the linear thermal dilatation coefficient α shown in the following equation,

$$h(T) = h_0(1 + \alpha T) \tag{12}$$

in which h_0 and h(T) respectively represent the thickness of the PDMS of the micro-mirror at an initial temperature T_0 and at temperature T.

We can show that the thermal action can be explicitly expressed as the efficacy of the coupling η(T) in Eq. (11) through the radius of curves bend R, by successively introducing Eq. (12) in Eq. (5), Eq. (5) in Eq. (10) and then Eq. (10) in Eq. (11).

Finally, the ratio of the reflected coupled light intensity is calculated taking into account the reflectance R_{refl} [87] as follows,

$$R_{refl}(T) = 10\log_{10}\left(\frac{P_r(T)}{P_i}\right) = 10\log_{10}(\eta(T)^2) \tag{13}$$

in which P_r is the reflected intensity and P_i the incident intensity. We then obtain

$$R_{refl}(T) = 20\log_{10}\left(\frac{2\omega_{01}(T)\omega_0}{\omega_{01}^2(T) + \omega_0^2}\right) \tag{14}$$

It can be noted that the maximum coupling is obtained when the waist $\omega_{01}(T)$ moves by distance $z = d - z_\omega$, and coincides with ω_0. These two parameters which modulate the efficacy of the coupling are calculated with respect to the temperature, and are represented in Fig. 5 below.

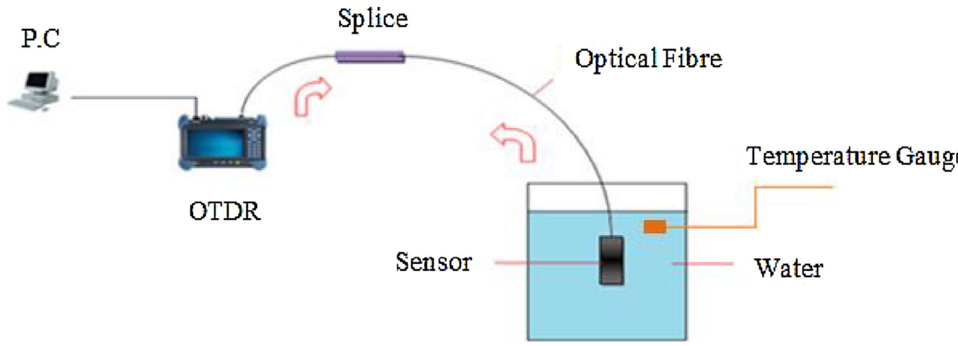

Fig. 6. Experimental setup of the sensor measurement and calibration with respect to the temperature.

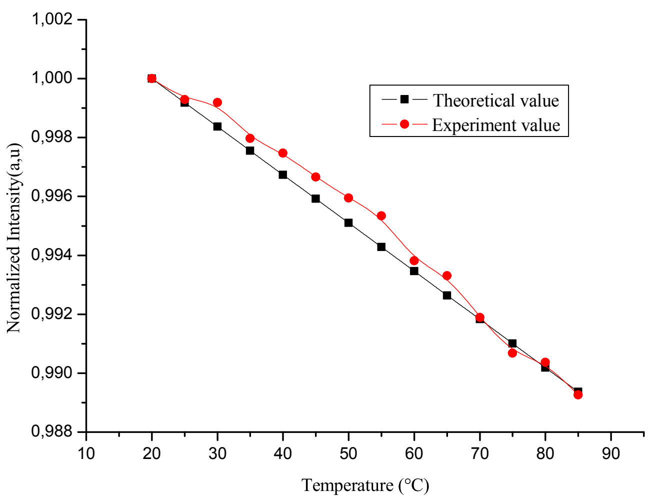

Fig. 7. Calculated and experimental curves showing the variation in light intensity with respect to the temperature.

These two curves show that when the temperature increases the waist image decreases and shifts away from the waist. Consequently, the optical coupling decreases, leading to a decrease in the reflected optical intensity to be measured.

4.2.1. Experimental results and discussions

The measurements of reflected light with respect to the thermal variation were obtained by the experimental setup shown in Fig. 6. The transmitter and receiver of the optical signal are built into the OTDR-type device, with a resolution of 0.01 dB, and operate at a wavelength of 1550 nm [88]. The 1.5 m long sensor is first spliced to the SMF fibre of the OTDR. It is then tested and calibrated in a temperature-controlled bath up to 100 °C.

The experimental results provided by the reflectometer (OTDR) with respect to the temperature are shown in Fig. 7. In addition, the theoretical calculation of the reflected luminous variation is obtained using Eq. 15. The corresponding curve is also shown in Fig. 7.

The theoretical curve and the experimental curve show a linear variation with respect to the given temperature of from 20 °C to 85 °C. They are defined by a correlation coefficient of $R = 0.9937$. Within this temperature range, the sensor's sensitivity is about -0.08dB/°C, with a resolution of 0.13°. The RMS error is around 0.01 dB.

4.3. Pressure effect on the coupling efficiency $\eta(P)$

This part is devoted to the study of the sensor's sensitivity with respect to pressure variation. To this end, the sensor was subjected to pressure stress in a device similar to that built by Paulo et al [20], and shown in Fig. 8. The device has an airtight chamber equipped with a manometer. The pressure chamber filled with distilled water is connected to a valve-controlled pressure pump. When the valve is opened the internal pressure varies and causes a deformation in the micro-mirror. Its bend radius increases when the pressure rises and decreases when the pressure falls. This variation acts on the coupling efficiency $\eta(P)$ of the reflected light intensity. The measurement of the reflected light is taken using the OTDR, in the same way as presented in the first part of this study.

5. Results and discussion

The action of the pressure on the micro-mirror is modelled using a study tool (COMSOL). Fig. 9 shows the deformation of the micro-mirror for a pressure variation of between 0 and 20 bars. The red and blue zones correspond, respectively, to the bend radius at 0 bars and at 20 bars as read on the manometer. The difference in pressure thus led to a displacement of the apex of the micro-mirror of 6 μm.

With respect to the previous analysis relative to the effect of the temperature on the coupling, pressure causes the reverse effect. Thus, if the pressure increases, the bend radius increases and the waist image $2\omega_{01}$ moves towards the front of the core of the fibre of the waist object $2\omega_0$. The maximum coupling is attained when these two waists coincide.

The dynamics of the sensor operation is shown in Fig. 10. The curve of the variation in the thickness of the micro-mirror, depending on the pressure applied, shows a linear variation. We can also see a linear variation in the reflected light intensity measured with respect to the pressure, on the one hand, and the consistency between the calculated curve and the experimental one, on the other hand.

The sensitivity of the sensor is around 0.11 dB/bar with a resolution of 0.09 bar. This value is consistent with the results obtained by other authors [71,72]. In addition, it is stable, with an RMS error of 0.009 dB. Linearity is relatively well characterised with a correlation coefficient (R) of 0.9979.

The error induced by the temperature on the pressure measurement is 1.38 bar/°C in cases in which there is no thermal compensation. And the error induced by the pressure on the temperature measurement is 0.72 °C/bar with no pressure compensation.

As mentioned above, the effect of temperature is opposite to that of pressure, these two quantities cannot be measured simultaneously. For a temperature less than or equal to 85 °C, the sensor

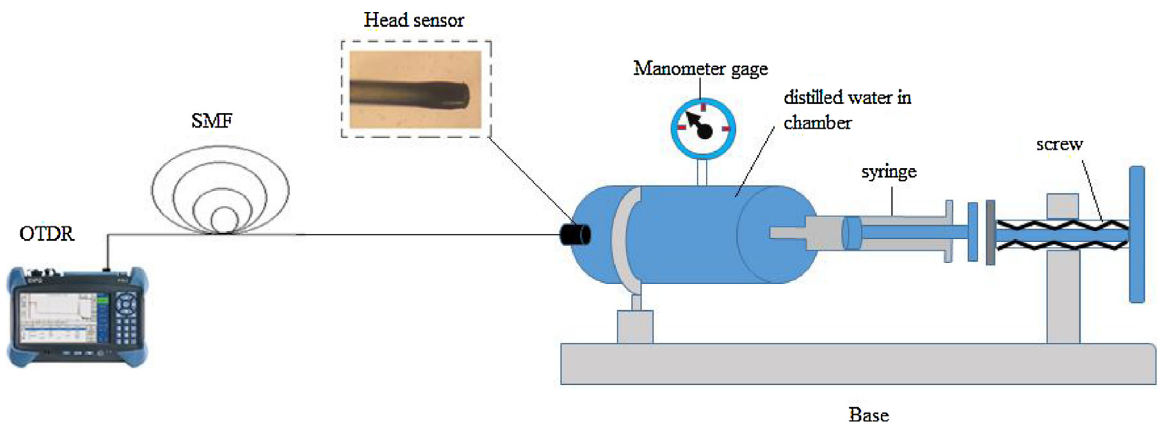

Fig. 8. Illustration of the principle showing the calibration of the sensor under pressure[20].

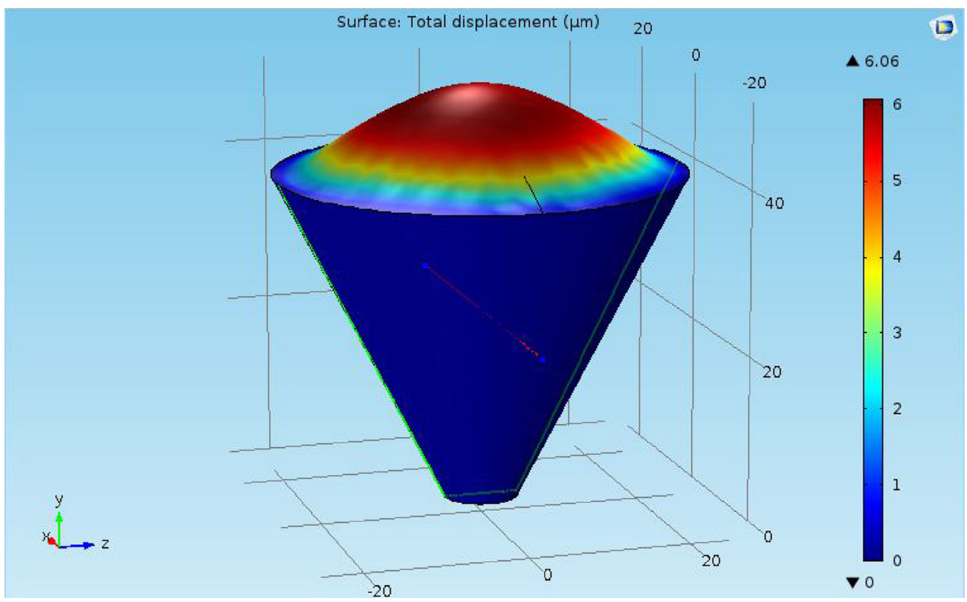

Fig. 9. 3D simulation by COMSOL illustrating the displacement of the apex of the micro-mirror. The maximum displacement at the centre is 6μm under pressure (20 bars).

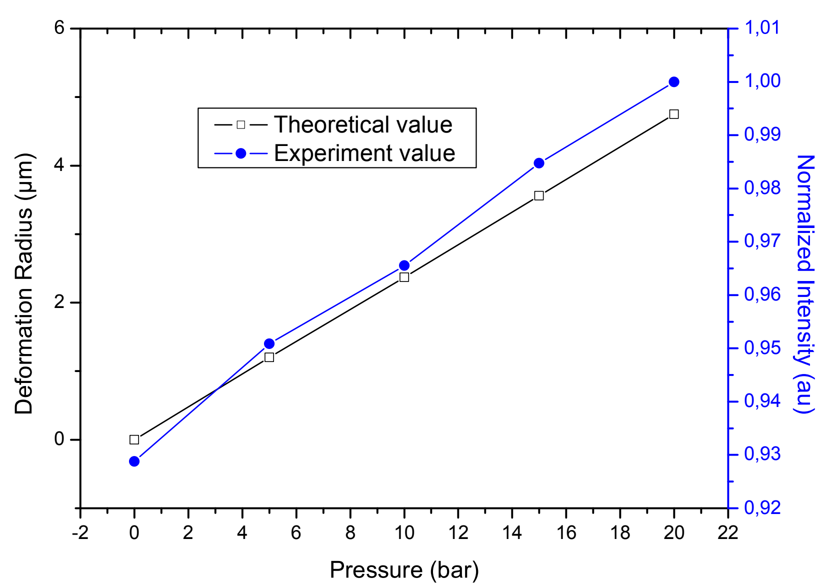

Fig. 10. Representation of the variation curve of the deformation of the micro-mirror with respect to the pressure, and the theoretical and experimental curves of the variation inthe reflected light.

is only sensitive to temperature. Beyond this temperature it works only in pressure sensor mode.

6. Conclusion

This study proposed an amplitude modulation sensor based on the use of a micro-mirror at the end of an optical fibre. This sensor is intended to measure the temperature and the pressure. The combinations between the bend radius of the concave micro-mirror and the angle of the cone opening may enable several sensors to be developed for specific uses. The sensor was calibrated for a temperature interval of from 20 °C to 85 °C. Its sensitivity was -0.08 dB/°C with a resolution of 0.13 °C. In this case the RMS error induced comes to 0.01 dB. Also, the sensor can be used to detect pressure ranging from 0 to 20 bars, with a sensitivity of 0.11 dB/bar and a resolution of 0.09 bars. The RMS error induced is equal to 0.009dB. In addition, it has been shown that there is low interaction between the two operating modes. However, it should be noted that the sensor becomes saturated at temperatures greater than 85 °C and therefore above this value the sensor will only operate in pressure mode. This sensor may be used in various areas of industrial application.

Acknowledgments

This work was sponsored by the Ministère de l'Enseignement Supérieur et de la Recherche scientifique MESRS, Algérie (Ministry of Higher Education and Scientific Research, Algeria) and by the Direction Générale de la Recherche Scientifique et du Développement Technologique DGRSDT, Algérie (General Directorate of Scientific Research and Technological Development, Algeria). The authors wish to express their sincere thanks to the Câbleries de Télécommunications d'Algérie CATEL, Algérie (Algerian Cable and Telecommunications Company, Algiers, Algeria) and the Centre d'Amplification CEL Algérie Télécom, Sétif, Algérie (Algeria Telecom CEL Amplification Centre, Setif, Algeria) for their collaboration.

References

[1] Byeong Ha Lee, Young Ho Kim, Kwan Seob Park, Joo Beom Eom, Myoung Jin Kim, Byung Sup Rho, Hae Young Choi, Interferometric fiber optic sensors, Sensors 12 (2012) 2467–2486.
[2] Byoungho Lee, Review of the present status of optical fiber sensors, Opt. Fiber Technol. 9 (2003) 57–79.
[3] Fabrizio Taffoni, Domenico Formica, Paola Saccomandi, Giovanni Di Pino, Emiliano Schena, Optical fiber-based MR-compatible sensors for medical applications: an overview, Sensors 13 (2013) 14105–14120.
[4] J. Jian Chen, Shih Chuan Liao, Mao Hsun Liu, Jenn Der Lin, Tsung Sheng Sheu, Ming Miao Jr, Surface tension flows inside surfactant-added poly(dimethylsiloxane) microstructures with velocity-dependent contact angles, Micromachines 5 (2014) 116–138.
[5] Marie Pospíšilov, Gabriela Kuncov, Josef Trögl, Fiber-optic chemical sensors and fiber-optic bio-sensors, Sensors 15 (2015) 25208–25259.
[6] Simon Pevec, Denis Donlagic, High resolution, all-fiber, micro-machined sensor for simultaneous measurement of refractive index and temperature, Opt. Express 22 (2014) 16241–16253.
[7] Jing Liu, Yuze Sun, Xudong Fan, Highly versatile fiber-based optical Fabry-Pérot gas sensor, Opt. Express 17 (2009) 2731–2738.
[8] Y.N. Ning, Z.P. Wang, A.W. Palmer, K.T.V. Grattan, Recent progress in optical current sensing techniques, Rev. Sci. Instrum. 66 (1995) 3097–3111.
[9] Yun-Jiang Rao, Recent progress in fiber-optic extrinsic Fabry–Perot interferometric sensors, Opt. Fiber Technol. 12 (2006) 227–237.
[10] Giuseppina Uva, Francesco Porco, Andrea Fiore, Giacinto Porco, Structural monitoring using fiber optic sensors of a pre-stressed concrete viaduct during construction phases, Case Stud. Nondestr. Test. Eval. 2 (2014) 27–37.
[11] Kunjian Cao, Yi Liu, Shiliang Qu, Highly sensitive temperature sensor based on cascaded polymer-microbubble cavities by employing a subtraction between reciprocal thermal responses, Opt. Express 24 (2016) 20655–20662.
[12] Xinpu Zhang, Wei Peng, Temperature-independent fiber salinity sensor based on Fabry-Perot interference, Opt. Express 23 (2015) 10353–10358.
[13] Iván Hernández-Romano, Miguel A. Cruz-Garcia, Carlos Moreno-Hernández, David Monzón-Hernández, Efraín O. López-Figueroa, Omar E. Paredes-Gallardo, Miguel Torres-Cisneros, Joel Villatoro, Optical fiber temperature sensor based on a microcavity with polymer overlay, Opt. Express 24 (2016) 5654–5661, http://dx.doi.org/10.1364/OE.24.005654.
[14] Ruohui Wang, Xueguang Qiao, Hybrid optical fiber Fabry–Perot interferometer for simultaneous measurement of gas refractive index and temperature, Appl. Opt. 53 (2014) 7724–7728.
[15] Wanfu Zheng, Jianglei Xie, Yi Li, Ben Xu, Juan Kang, Changyu Shen, Jianfeng Wang, Yongxing Jin, Honglin Liu, Kai Ni, Xinyong Dong, Chunliu Zhao, Shangzhong Jin, A fiber air-gap Fabry–Pérot temperature sensor demodulated by using frequency modulated continuous wave, Opt. Commun. 324 (2014) 234–237.
[16] Chao Chen, Yong-Sen Yu, Xuan-Yu Zhang, Rui Yang, Cong-Cong Zhu, Chuang Wang, Yang Xue, Feng Zhu, Qi-Dai Chen, Hong-Bo Sun, Compact fiber tip modal interferometer for high-temperature and transverse load measurements, Optics Letters. 38 (2013) 3202–3204.
[17] Hae Young Choi, Kwan Seob Park, Seong Jun Park, Un-Chul Paek, Byeong Ha Lee, Eun Seo Choi, Miniature fiber-optic high temperature sensor based on a hybrid structured, Optics Letters. 33 (2008) 2455–2457.
[18] Chunliu Zhao, Binqing Wu, Feifei Shi, Juan Kang, Dongning Wang, Simultaneous measurement of trace organic vapors and temperature by use of zeolite thin film-coated fiber spherical end face and fiber Bragg grating, Optical Engineering. 56 (2017) 0361171–0361175.
[19] Daniele Tosi, Paola Saccomandi, Emiliano Schena, Dinesh Babu Duraibabu, Sven Poeggel, Gabriel Leen, Elfed Lewis, Intra-tissue pressure measurement in ex vivo liver undergoing laser ablation with fiber-optic fabry-perot probe, Sensors 16 (2016) 1–11.
[20] Paulo Roriz, João M.C. Ferreira, JoséC. Potes, Maria T. Oliveira, Orlando Frazão, José Luís Santos, José António de Oliveira Simões, In vivo measurement of the pressure signal in the intervertebral disc of an anesthetized sheep, J. Biomed. Opt. 19 (2014) 1–6.
[21] H. Bae, M. Yu, Miniature Fabry-Perot pressure sensor created by using UV-molding process with an optical fiber based mold, Opt. Express 20 (2012) 14573–14583.
[22] Dinesh Babu Duraibabu, Sven Poeggel, Edin Omerdic, Romano Capocci, Elfed Lewis, Thomas Newe, Gabriel Leen, Daniel Toal, Gerard Dooly, An optical fibre depth (pressure) sensor for remote operated vehicles in underwater applications, Sensors 17 (2017) 1–12.
[23] Yizheng Zhu, Kristie L. Cooper, Gary R. Pickrell, Anbo Wang, High-temperature fiber-tip pressure sensor, J. Lightwave Technol. 24 (2006) 861–869, http://dx.doi.org/10.1109/jlt.2005.862444.
[24] Stuart Watson, Matthew J. Gander, William N. MacPherson, James S. Barton, Julian D.C. Jones, Thomas Klotzbuecher, Torsten Braune, Johannes Ott, Felix Schmitz, Laser-machined fibers as Fabry–Perot pressure sensors, Appl. Opt. 45 (2006) 5590–5596.
[25] Qi Wang, Dongchao Yan, Binbin Cui, Zixuan Guo, Optimal design of an hourglass in-fiber air Fabry-Perot microcavity—towards spectral characteristics and strain sensing technology, Sensors 17 (2017) 1–12.
[26] Jitendra Narayan dash, Rajan Jha, Fabry–Perot based strain insensitive photonic crystal fiber modal interferometer for inline sensing of refractive index and temperature, Appl. Opt. 54 (2015) 10479–10486.
[27] Ye Liu, D.N. Wang, W.P. Chen, Crescent shaped Fabry-Perot fiber cavity for ultra-sensitive strain measurement, Scientific Reports. 6 (2016) 1–9.
[28] Shen Liu, Yiping Wang, Changrui Liao, Guanjun Wang, Zhengyong Li, Qiao Wang, Jiangtao Zhou, Kaiming Yang, Xiaoyong Zhong, Jing Zhao, Jian Tang, High-sensitivity strain sensor based on in-fiber improved Fabry–Perot interferometer, Opt. Lett. 39 (2014) 2121–2124.
[29] Chenchen Yin, Zhigang Cao, Zhao Zhang, Tao Shui, Rui Wang, Jian Wang, Liang Lu, Shenglai Zhen, Yu Benli, Temperature-independent ultrasensitive Fabry–Perot all-fiber strain sensor based on a bubble-expanded microcavity, IEEE Photon. J. 6 (2014), http://dx.doi.org/10.1109/JPHOT.2014.2345883, 1943-0655.
[30] Paula A.R. Tafulo, P.A.S. Jorge, J.L. Santos, O. Frazão, Fabry–Pérot cavities based on chemical etching for high temperature and strain measurement, Opt. Commun. 285 (2012) 1159–1162.
[31] Xuefeng Li, Yujiao Shao, Yuan Yu, Yin Zhang, Shaowen Wei, A highly sensitive fiber-optic Fabry–Perot interferometer based on internal reflection mirrors for refractive index measurement, Sensors 16 (2016) 1–12.
[32] Chuang Wu, Zhengyong Liu, A. Ping Zhang, Bai-Ou Guan, Hwa-Yaw Tam, In-line open-cavity Fabry–Pérot interferometer formed by C-shaped fiber for temperature insensitive refractive index sensing, Opt. Express 22 (2014) 21757–21766.
[33] Ming Tian, Ping Lu, Li Chen, Deming Liu, Minghong Yang, Jiangshan Zhang, Femto second laser fabricated in-line micro multicavity fiber FP interferometers sensor, Opt. Commun. 316 (2014) 80–85.
[34] Zhitao Cao, Lan Jiang, Sumei Wang, Peng Wang, Fei Zhang, Yongfeng Lu, Trench-embedding fiber taper sensor fabricated by a femtosecond laser for gas refractive index sensing, Appl. Opt. 53 (2014) 1028–1032.
[35] Shecheng Gao, Weigang Zhang, Hao Zhang, Pengcheng Geng, Wei Lin, Bo Liu, Zhiyong Bai, Xiaolin Xue, Fiber modal interferometer with embedded fiber Bragg grating for simultaneous measurements of refractive index and temperature, Sens. Actuators B 188 (2013) 931–936.
[36] Guolu Yin, Shuqin Loun, Hui Zou, Refractive index sensor with asymmetrical fiber Mach–Zehnder interferometer based on concatenating single-mode abrupt taper and core-offset section, Opt. Laser Technol. 45 (2013) 294–300.
[37] Jinpeng Yang, Lan Jiang, Sumei Wang, Qianghua Chen, Benye Li, Hai Xiao, Highly sensitive refractive index optical fiber sensors fabricated by a femtosecond laser, IEEE Photon. J. 3 (2011) 1189–1197.

[38] Tingting Gang, Manli Hu, Qiangzhou Rong, Xueguang Qiao, Lei Liang, Nan Liu, Rongxin Tong, Xiaobo Liu, Ce Bian, High-frequency fiber-optic ultrasonic sensor using air micro-bubble for imaging of seismic physical models, Sensors 16 (2016) 1–10.
[39] Jinyu Ma, Meirong Zhao, Xinjing Huang, Hyungdae Bae, Yongyao Chen, Miao Yu, Low cost, high performance white-light fiber optic hydrophone system with a trackable working point, Opt. Express 24 (2016) 19008–19019.
[40] Xiaotian Zou, Nan Wu, Ye Tian, Xingwei Wang, Broadband miniature fiber optic ultrasound generator, Opt. Express 22 (2014) 18119–18127.
[41] Sulaiman Wadi Harun, H.Z. Yang, Moh Yasin, H. Ahmad, Theoretical and experimental study on the fiber optic displacement sensor with two receiving fibers, Microw. Opt. Technol. Lett. 52 (2010) 373–375.
[42] Vijay K. Kulkarni, Anandkumars Lalasangi, I.I. Pattanashetti, U.S. Raikar, Fiber optic micro-displacement sensor using coupler, J. Optoelectr. Adv. Mater. 8 (2006) 1610–1612 https://joam.inoe.ro/arhiva/vol8nr4.html.
[43] D. Milewsk, K. Karpienk, M. Jędrzejewska-Szczersk, Application of thin diamond films in low-coherence fiber-optic Fabry Pérot displacement sensor, Diam. Relat. Mater. 64 (2016) 169–176.
[44] Nur Izzati Ismail, Nor Hafizah Ngajikin, Nor Fadzlina Mohd Zaman, Maisarah Awang, Asrul Izam Azmi, Nik Noordini Nik Abd. Malik, Norazan Mohd Kassim, Resolution improvement in Fabry-Perot displacement sensor based on fringe counting method, Telkomnika 12 (2014) 811–818.
[45] H.-Z. Yang, X.-G. Qiao, K.-S. Lim, S.W. Harun, W.-Y.C.R. Islam, H. Ahmad, Optical fiber sensing of salinity and liquid level, IEEE Photonics Technology Letters 26 (2014) 1742–1745.
[46] Yun-Long Bai, Bin Yin, Yan-Hui Qi, You-Chao Jiang, Yue Wu, Shui-Sheng Jian, Simultaneous measurement of pressure and temperature based on processed capillary tube and fiber Bragg grating, Opt. Eng. 55 (2016) 080502–080504.
[47] Yaxun Zhang, Yu Zhang, Zhenzhen Wang, Zhihai Liu, Yong Wei, Enming Zhao, Xinghua Yang, Jian zhong Zhang, Jun Yang, Libo Yuan, A novel Michelson Fabry–Perot hybrid interference sensor based on the micro-structured fiber, Opt. Commun. 374 (2016) 58–63.
[48] Li Duan, Peng Zhang, Ming Tang, Ruoxu Wang, Zhiyong Zhao, Songnian Fu, Lin Gan, Benpeng Zhu, Weijun Tong, Deming Liu, Perry Ping Shum, Heterogeneous all-solid multicore fiber based multipath Michelson interferometer for high temperature sensing, Opt. Express 24 (2016) 20210–20218.
[49] Zhengyong Li, Changrui Liao, Yiping Wang, Lei Xu, Dongning Wang, Xiaopeng Dong, Shen Liu, Qiao Wang, Kaiming Yang, Jiangtao Zhou, Highly-sensitive gas pressure sensor using twincore fiber based in-line Mach-Zehnder interferometer, Opt. Express 23 (2015) 6673–6678.
[50] Ai Zhou, Yaxun Zhang, Quan Xu, Jun Yang, Libo Yuan, Semi-open cavity in-fiber Mach–Zehnder interferometer for temperature measurement with ultra-high sensitivity, 20 April, Appl. Opt. 53 (2014) 2696–2701.
[51] Ming Han, Fawen Guo, Yongfeng Lu, Optical fiber refractometer based on cladding-mode Bragg grating, Opt. Lett. 35 (2010) 399–401.
[52] Cheng Zhang, Junfa Zhao, Changyun Miao, Hongqiang Li, Hua Bai, Meiling Zhang, Curvature and temperature sensor based on bulge-taper structures interferometer with embedded fiber Bragg grating, Optical Engineering 54 (2015) 1–6.
[53] Jiajun tian, Lu Zejin, Mingran Quan, Yuzhu Jiao, Yong Yao, Fast response Fabry–Perot interferometer microfluidic refractive index fiber sensor based on concave-core photonic crystal fiber, Opt. Express 24 (2016) 20132–20142.
[54] Shaolin Zhang, Ziwen Zhao, Na Chen, Fufei Pang, Zhenyi Chen, Yunqi Liu, Tingyun Wang, Temperature characteristics of silicon core optical fiber Fabry–Perot interferometer, Optics Letters. 40 (2015) 1362–1365.
[55] C.E. Lee, H.F. Taylor, A.M. Markus, E. Udd, Optical-fiber Fabry-Perot embedded sensor, Opt. Lett. 14 (1989) 1225–1227.
[56] Linghao Cheng, Cengzhong Wang, Yunyun Huang, Hao Liang, Bai-ou Guan, Silk fibroin diaphragm-based fiber-tip Fabry-Perot pressure sensor, Opt. Express 24 (2016) 19600–19606.
[57] G.C. Hill, R. Melamud, F.E. Declercq, A.A. Davenport, I.H. Chan, P.G. Hartwell, B.L. Pruitt, SU-8 MEMS Fabry-Perot pressure sensor, Sens. Actuators A 138 (2007) 52–62.
[58] A.D. Gaikwad, J.P. Gawande, A.K. Joshi, R.H. Chile, an intensity-modulated optical fiber sensor with concave mirror for measurement of displacement, J. Opt. 42 (2013) 300–306.
[59] Ai Zhou, Zhihai Liu, Libo Yuan, Fiber-optic dipping liquid analyzer: theoretical and experimental study of light transmission, Appl. Opt. 48 (2009) 6928–6933.
[60] H.Z. Yang, S.W. Harun, H. Ahmad, Theoretical and experimental studies on concave mirror-based fiber optic displacement sensor, Sens. Rev. 31 (2011) 65–69.
[61] S.W. Harun, M. Yasin, H.A. Rahman, H. Arof, H. Ahmad, Fiber Optic Temperature Sensors, Optical Fiber Communications and Devices, InTech, China, 2012, pp. 362–380, http://dx.doi.org/10.5772/2427.
[62] H.Z. Yang, K.S. Lim, S.W. Harun, K. Dimyati, H. Ahmad, Enhanced bundle fiber displacement sensor based on concave mirror, Sens. Actuators A 162 (2010) 8–12.
[63] Chen Yang, S. Olutunde Oyadiji, Development of two-layer multiple transmitter fibre optic bundle displacement sensor and application in structural health monitoring, Sens. Actuators A 244 (2016) 1–14.
[64] Thunter Hwang, Wood-Hi Cheng, Yan-Kuin Su, Characteristics and applications of tapered fiber optical sensors for 1310nm wavelength, Jpn. J. Appl. Phys. 52 (2013) 062503–062505.
[65] Xuan-Yu Zhang, Cong-Cong Zhu, Chao Chen, Rui Yang, Yang Xue, H.-B.S. Qi-Dai Chen, Miniature end-capped fiber sensor for refractive index and temperature measurement, IEEE Photon. Technol. Lett. 26 (2014) 7–10.
[66] Min Li, Fiber-optic sensor tip for measuring temperature and liquid refractive index, Opt. Eng. 53 (2014) 1–5.
[67] X.L. Tan, Y.F. Geng, X.J. Li, Y.L. Deng, Z. Yin, R. Gao, UV-curable polymer micro hemisphere-based fiber-optic Fabry-Perot interferometer for simultaneous measurement of refractive index and temperature, IEEE Photon. J. 6 (2014) 1–8, http://dx.doi.org/10.1109/JPHOT.2014.2332460.
[68] Jing Kong, Ai Zhou, Libo Yuan, Temperature insensitive one-dimensional bending vector sensor based on eccentriccore fiber and air cavity Fabry-Perot interferometer, J. Opt. 19 (2017) 045705, http://dx.doi.org/10.1088/2040-8986/aa535b, 5pp.
[69] Shen Liu, Yiping Wang, Changrui Liao, Ying Wang, Jun He, Cailing Fu, Kaiming Yang, Zhiyong Bai, Feng Zhang, Nano silica diaphragm in fiber cavity for gas pressure measurement, Sci. Rep. 7 (2017) 1–9.
[70] W.P. Chen, D.N. Wang, Ben Xu, C.L. Zhao, H.F. Chen, Multimode fiber tip Fabry-Perot cavity for highly sensitive pressure measurement, Scientific Reports. 7 (2017) 1–6.
[71] Ben Xu, Chao Wang, D.N. Wang, Yaming Liu, Yi Li, Fiber-tip gas pressure sensor based on dual capillaries, Optics Express. 23 (2015) 23484–23492.
[72] B. Sun, Y. Wang, J. Qu, C. Liao, G. Yin, J. He, J. Zhou, J. Tang, S. Liu, Z. Li, Y. Liu, Simultaneous measurement of pressure and temperature by employing Fabry-Perot interferometer based on pendant polymer droplet, Opt. Express 23 (2015) 1906–1911.
[73] Husna Abdul Rahman, Sulaiman Wadi Harun, Norazlina Saidin, Moh. Yasin, Harith Ahmad, Fiber optic displacement sensor for temperature measurement, IEEE Sens. J. 12 (2012) 1361–1364.
[74] S.W. Harun, H.Z. Yang, K.S. Lim, M.R. Tamjis, K. Dimyati, H. Ahmad, Fiber optic displacement sensor based on concave mirror, Optoelectr. Adv. Mater. – Rapid Commun. 3 (11) (2009) 1139–1141, ISSN: 1842-6573 http://www.journals4free.com/link.jsp?l=13673897).
[75] Nacer-Eddine Demagh, Assia Guessoum, Hind Aissat, Chemical etching of concave cone fibre ends for core fibres alignment, Meas. Sci. Technol. 17 (2006) 119–122, http://dx.doi.org/10.1088/0957-0233/17/1/019.
[76] Monsef Zaboub, Assia Guessoum, Nacer-Eddine Demagh, Abdelhak Guermat, Fabrication of polymer microlenses on single mode optical fibers for light coupling, Opt. Communs. 366 (2016) 122–126.
[77] Xiaotian Zou, Nan Wu, Ye Tian, Yang Zhang, Xingwei Wang, Polydimethylsiloxane thin film characterization using all-optical photoacoustic mechanism, Appl. Opt. 52 (2013) 6239–6244.
[78] Xiaotian Zou, Broadband miniature fiber optic ultrasound generator, Opt. Express 22 (2015) 18119–18127.
[79] Jinyu Ma, Meirong Zhao, Xinjing Huang, Hyungdae Bae, Yongyao Chen, Miao Yu, Low cost, high performance white-light fiber optic hydrophone system with a trackable working point, Opt. Express 24 (2016) 19008–19019.
[80] Carlos Moreno-Hernández, David Monzón-Hernández, Iván Hernández-Romano, Joel Villatoro, Single tapered fiber tip for simultaneous measurements of thickness, refractive index and distance to a sample, Optics Express. 23 (2015) 22141–22148.
[81] J.C. Lotters, W. Olthuis, P.H. Veltink, P. Bergveld, The mechanical properties of the rubber elastic polymer polydimethylsiloxane for sensor applications, J. Micromech. Microeng. 7 (1997) 145–147.
[82] E. Li, Characterization of a fiber lens, Opt. Lett. 31 (2006) 169–171.
[83] H.Z. Liu, the approximate ABCD matrix for a parabolic lens of revolution and its application in calculating the coupling efficiency, Optik 119 (2008) 666–670.
[84] D. Marcuse, Gaussian approximation of the fundamental modes of graded-index fibers, J. Opt. Soc. Am. 68 (1978) 103–109.
[85] Herwig Kogelnik, On the propagation of Gaussian beams of light through Lens like media including those with a loss or gain variation, Appl. Opt. 4 (1965) 1562–1568.
[86] Wl. Emkey, C.A. Jack, Analysis and evaluation of graded-index fiber-lenses, J. Light Wave Technol. 5 (1987) 1156–1164.
[87] X. Zhou, Z. Chen, Z. Wang, J. Hou, Monolithic fiber end cap collimator for high-power free-space fiber–fiber coupling, Appl. Opt. 55 (2016) 4001–4004.
[88] Edvard Cibula, Denis Donlagic, In-line short cavity Fabry-Perot strain sensor for quasi distributed measurement utilizing standard OTDR, Opt. Express 15 (2007) 8719–8730.

Biographies

Abdelhak Guermat received his MSc degree (2007) in Optics and Precision Mechanics from Ferhat ABBAS University Setif 1, Algeria. His research is focused on fibre optic sensors.

Assia Guessoum received her PhD (2013) in Optics and Precision Mechanics from Ferhat ABBAS University Setif1, Algeria. Currently, she is a lecturer at the Institute of Optics and Precision Mechanics. Her research interests include fibre optic micro-collimators and optical metrology.

Nacer-Eddine Demagh obtained his PhD (1986) from ULP Strasbourg University, France. He is a professor at the Institute of Optics and Precision Mechanics of Ferhat ABBAS University Setif 1, Algeria. His current research interest is in fibre optic sensors and micro-lensed optical fibres.

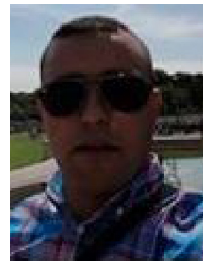

Monsef Zaboub received his PhD of science (2016) in Optics and Precision Mechanics from Ferhat ABBAS University Setif 1, Algeria. His research is focused on micro-collimators.

Zaied Bouhafs received his Master of Science (2012) in Optics and Precision Mechanics from Ferhat ABBAS University Setif 1, Algeria. He is currently working towards the PhD. His research is focused on parabolic micro-lens.